Lt. Gregory R. Mitchell, USN; Dr. Robert W. Cox; James Paris; Dr. Steven B. Leeb

Shipboard Fluid System Diagnostic Indicators Using Non-Intrusive Load Monitoring

ABSTRACT

Field studies have demonstrated that it is possible to evaluate the state of many shipboard systems by analyzing the electrical power that is drawn by electromechanical actuators (Ramsey et al. 2005, DeNucci et al. 2005, Cox et al. 2006, Cox et al. 2007). This paper demonstrates how a device known as a non-intrusive load monitor (NILM) uses only electrical power data to detect several critical faults in shipboard fluid systems. Using the example of reverse-osmosis units installed aboard the US Coast Guard's Medium Endurance Cutters, it is shown that the NILM can provide ship's force with a highly reliable real-time system monitoring capability.

INTRODUCTION

Modern naval vessels are becoming increasingly dependant on electrical systems. One example of this trend is the replacement of distilling and evaporator plants with reverse-osmosis (RO) units. Because of the pressure to reduce shipboard manning, these new systems often feature automated monitoring and diagnostic capabilities. In order to accurately assess system conditions, these diagnostic tools typically require a number of sensors. Large sensor networks are undesirable, however, because they are difficult to install and maintain.

One diagnostic platform that is particularly well suited for use aboard modern naval vessels is the non-intrusive load monitor (NILM). The primary benefit of the NILM is that it can assess the operational status of multiple electrical loads from a single set of measurements collected at a central point in a ship's power-distribution network (Leeb et al. 1995, Cox et al. 2007). This reduction in sensor count makes the NILM a low cost and highly reliable system.

System modeling, laboratory experiments, and field studies conducted aboard two USCG Medium Endurance Cutters have all demonstrated that the NILM can effectively detect and diagnose several critical faults in shipboard fluid systems. This paper focuses on the development of a field-tested, model-based method that can be used to detect filter clogging in reverse-osmosis units. Cox et al. (2007) discusses the detection of several other faults in the RO system.

Following a brief description of the NILM itself, this paper summarizes reverse-osmosis operation and presents a model that describes the inter-domain interactions that occur during startup. The paper subsequently discusses several laboratory experiments and it provides results from several field tests performed aboard the *USCGC Seneca* and the *USCGC Escanaba*.

NILM OVERVIEW

Figure 1 shows the block diagram of a standard NILM. Note that the NILM measures the aggregate current flowing to a bank of electrical loads. Using these measurements the NILM is able to disaggregate the operating schedule of individual loads. In an engineering plant the candidate installation locations include generator output busses and distribution panels.

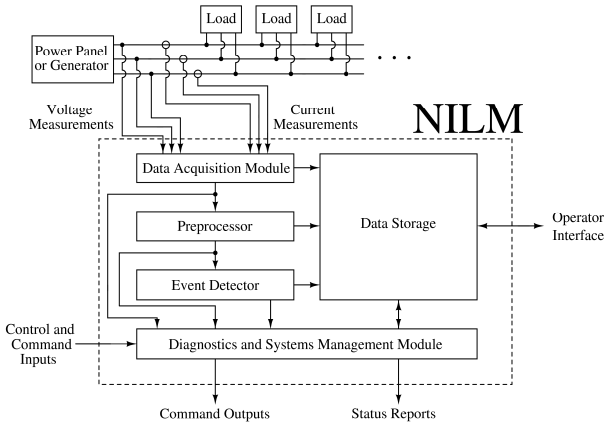

FIGURE 1. Diagram showing the fundamental signal flow path in a NILM.

Using measurements of the line voltage and aggregate current, a software-based preprocessor onboard the NILM computes time-varying estimates of the frequency content of the measured line current (Shaw 2000). Formally, these time-varying estimates, or spectral envelopes, are defined as the quantities (Shaw et al. 1998)

$$a_m(t) = \frac{2}{T}\int_{t-T}^{t} i(\tau)\sin(m\omega\tau)\,d\tau \qquad (1)$$

and

$$b_m(t) = \frac{2}{T}\int_{t-T}^{t} i(\tau)\cos(m\omega\tau)\,d\tau\,. \qquad (2)$$

These equations are Fourier-series analysis equations evaluated over a moving window of length T (Oppenheim et al. 1988). The coefficients $a_m(t)$ and $b_m(t)$ contain time-local information about the frequency content of $i(t)$. Provided that the basis terms $\sin(m\omega t)$ and $\cos(m\omega t)$ are synchronized to the line voltage, the spectral envelope coefficients have a useful physical interpretation as real, reactive, and harmonic power (Leeb et al. 1995).

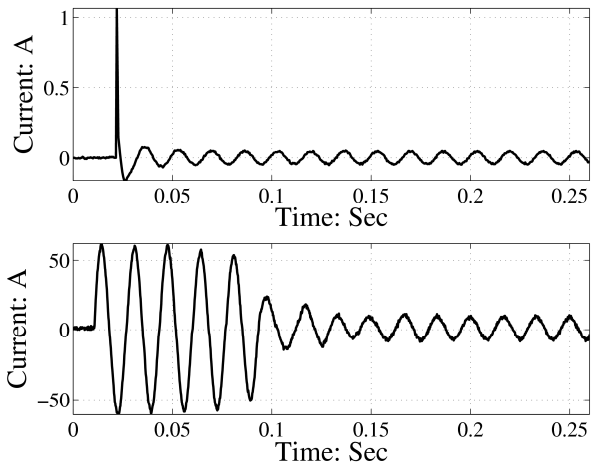

FIGURE 2. Top trace: Current drawn during the start of an incandescent lamp. Bottom trace: Stator current drawn during the start of an unloaded, fractional horsepower induction machine.

The spectral envelopes computed by the preprocessor are passed to an event detector that identifies the operation of each of the major loads. In a modern NILM, identification is performed using both transient and steady-state information (Lee 2003). Field studies have demonstrated that transient details are particularly powerful because the transient electrical behavior of a particular load is strongly influenced by the physical task that is performed (Leeb 1995). As shown in Fig. 2, for example, the physical differences between an incandescent lamp and an induction machine result in vastly different transient patterns. Figure 3 demonstrates the positive identification of an induction motor driving a small vacuum pump. Further details of the detection and identification process can be found in Lee (2003) and Leeb (1993).

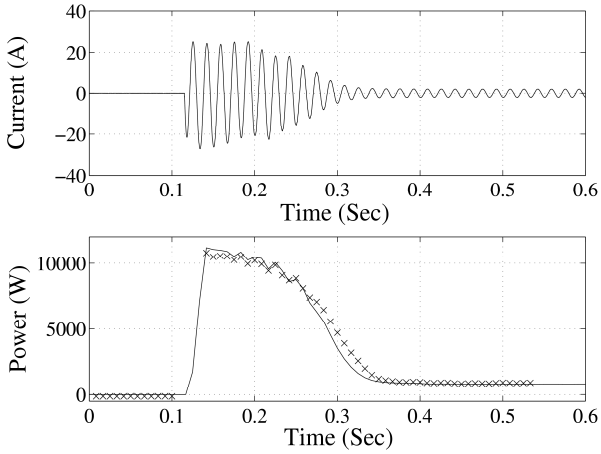

FIGURE 3. Measured current and computed power during the start of 1.7hp vacuum pump motor. Also shown in the power plot is a section of the template that has been successfully matched to the observed transient behavior by the NILM's event detector.

The final block in Fig. 1 is the NILM's diagnostics and systems management module. This software unit assesses load status using any required combination of current data, voltage data, spectral envelopes, and load operating schedules (Cox 2006). The successful application of this module has been demonstrated in numerous publications (Armstrong et al. 2006; Cox et al. 2006; Cox et al. 2007; DeNucci et al. 2005; Laughman et al. 2006; Lee 2003; Shaw 2000). Shipboard applications are highlighted in DeNucci et al. (2005), Cox et al. (2006), and Cox et al. (2007).

REVERSE-OSMOSIS SYSTEM MODEL

Many modern vessels produce desalinated water via reverse osmosis. In this process a large differential pressure is imposed across a semi-permeable membrane that has brackish water on one side and fresh water on the other. The high differential pressure, which is typically in the range of 750 to 1200 psi, forces water to pass from the diluted solution (Zarambo 1992).

Figure 4 is a simplified schematic of the reverse-osmosis units on the USCG's Medium Endurance Cutters. In those units, saltwater from the Sea Chest is vertically lifted by a small centrifugal pump known as the low-pressure (LP) pump. Once lifted, the incoming feedwater separates into two paths. After passing through a series of pretreatment filters, water in each path is raised to a high pressure by a positive-displacement pump. Each of these high-pressure (HP) pumps discharges into several membranes that separate the seawater into brine and potable water. On both the *Escanaba* and the *Seneca*, a NILM currently monitors the aggregate current flowing to all three pumps. Figure 5 shows the power drawn during a typical system start.

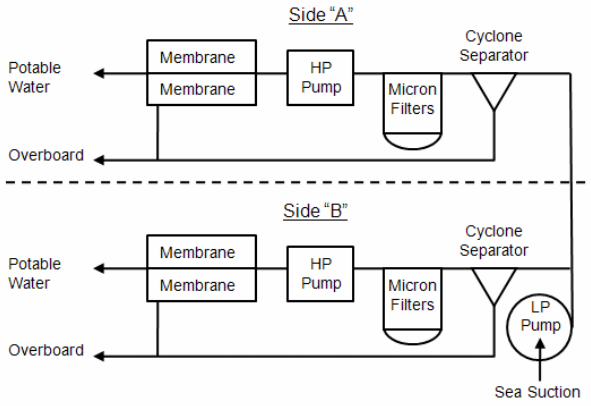

FIGURE 4. Simplified schematic of the reverse-osmosis system aboard a USCG Medium Endurance Cutter. Note that the cyclone separator can discharge water overboard. All three pumps are monitored by the same NILM.

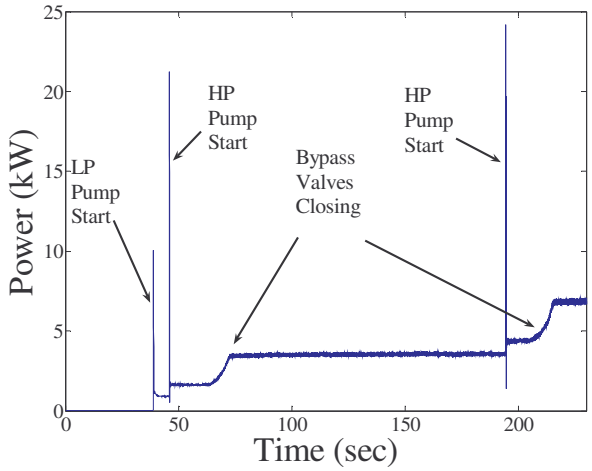

FIGURE 5. Power drawn by the pumps in the RO unit during a typical system start. Note that manual valve throttling causes a change in the steady-state power.

Contamination can have a catastrophic effect on the positive-displacement pumps in an RO system. Aboard the Cutters, most contaminants are removed by the actions of the cyclone separators and the micron filters (Village Marine 2004). As shown in Fig. 4, the separators pass a certain amount of fluid overboard. This ejected water contains most of the suspended solids found in the incoming feed water. Any remaining particulates with diameters greater than 5μm are removed by the subsequent micron filters (Village Marine 2004). Over time, the filters clog, thus increasing the pressure loss across the filters and decreasing the absolute pressure at the inlets of the positive-displacement pumps. Because the loss in inlet pressure can result in harmful cavitation, the filters must be routinely cleaned or replaced. To assess filter status, watch standers check the pressure across the filters each hour. To avoid human errors, relieve watch stander burden, and prevent sudden failures in highly contaminated waters, it is desirable to assess filter status using automated procedures.

One way to detect filter clogging in real time is to examine electrical power data. Robust, model-based detection methods can be developed by considering the inter-domain interactions that occur during a system start. As shown in Fig. 5, the centrifugal (LP) pump is the first device to be energized. While that pump is running by itself, it is solely responsible for pushing fluid through the

micron filters and the overboard discharge. Thus, as the filter volume fills with water, the state of the filter has a strong effect of the flow rate, which in turn impacts the current drawn by the pump motor. By comparison, the filters have little effect once the HP pumps come online because these positive-displacement pumps impose a relatively constant flow rate through the filters (Volk 2005). Thus, during the initial charging period, there is a unique opportunity to probe the effects of a change in the state of the micron filters.

A relatively simple model can be formulated to describe the salient features of the pump-fluid interactions that occur during the initial charging phase. Essentially, the centrifugal pump is creating the pressure difference necessary to move fluid through the cyclone separators and the micron filters. To a reasonable approximation, this means that the pump is driving fluid through a long pipe that eventually splits, providing some water to the filters and some to the overboard discharge path. In both the piping that follows the pump and the piping that carries discharged water overboard, one can approximate the head loss, $h(t)$, using the relation

$$h(t) = \frac{l}{gA}\frac{dQ}{dt} + f(Q), \tag{3}$$

where $Q(t)$ is the volumetric flow rate, g is the gravitational constant, l is the length of the pipe, A is the cross-sectional area, and $f(Q)$ is a function representing energy loss due to the resistance of the pipe (Isermann 2006, Wolfram et al. 2001, Wood et al. 2005, Munson et al. 1998). This relationship, which considers only bulk fluid motion in the axial direction, is a simplification that accounts for inertial effects and energy loss. The loss term in Eq. 3 is typically approximated using the relation

$$f(Q) = kQ^2, \tag{4}$$

where k is a constant that depends on both the geometry and properties of the pipe as well as the properties of the flowing fluid (Isermann 2006, Wolfram et al. 2001, Munson et al. 1998, Hogan 1989).

During an initial start, the filter housing slowly fills wither water. As the volume fills, the amount of stored head increases. Assuming that there is a linear relationship between head and volume, the constitutive relation for this device is

$$h = CV, \tag{5}$$

where V is the amount of water stored in the housing and C is a constant. In direct analogy with electrical systems, this device can be viewed as a capacitor. Although this model simplifies the actual physics, it does capture the salient characteristics of the filter and it is often used in similar models (Hogan 1989). Assuming that C does not vary as a function of time, the flow rate through the device can be determined using the following relationship

$$\frac{dh}{dt} = C\frac{dV}{dt} = CQ. \tag{6}$$

The above arguments can be used to produce an overall model for the fluid subsystem. The model contains three states: the pump discharge capacity (Q_{IN}), the flow rate in the overboard discharge piping (Q_{DIS}), and the head across the filters (h_{OUT}). Neglecting any head loss in the piping ahead of the filters, it can be assumed that the filters and the discharge piping form two parallel paths with the same overall head loss, h_{OUT}. Assuming that compressibility is negligible, the continuity equation shows that

$$Q_{IN}(t) = Q_{DIS}(t) + Q_{FIL}(t), \tag{7}$$

where Q_{FIL} is the rate at which water flows through the micron filters. The three state equations in the model are the following:

$$h_{IN}(t) = \alpha_{IN}\frac{dQ_{IN}}{dt} + k_{IN}Q_{IN}^{\ 2}, \tag{8}$$

$$h_{OUT}(t) = \alpha_{DIS}\frac{dQ_{DIS}}{dt} + k_{DIS}Q_{DIS}^{\ 2}, \tag{9}$$

and

$$C\frac{dh_{OUT}}{dt} = Q_{FIL}(t) = Q_{IN}(t) - Q_{DIS}(t). \tag{10}$$

In this model, Eq. 8 describes the bulk motion of the fluid that is expelled by the pump, Eq. 9 describes the bulk motion of the fluid in the discharge piping and Eq. 10 models the flow through the micron filters. The constants used in these equations are summarized in Table 1.

TABLE 1: Constants used in Eqs. 8 - 10.

Parameter	Definition
α_{IN}	Inertial coefficient related to the pump discharge piping
k_{IN}	Loss coefficient in pump discharge piping
α_{DIS}	Inertial coefficient related to the overboard discharge piping
k_{DIS}	Loss coefficient in overboard discharge piping
C	Fluid capacitance associated with the micron filters.

The remainder of the overall model must account for the mechanics of the centrifugal pump and the dynamics of the motor that drives it. Such pumps produce an output head that exhibits a nonlinear dependence on both speed and flow. The salient characteristics of this dependence are captured using the relationship

$$h_{IN}(t) = a_1\omega_r^2 + a_2\omega_r Q_{IN} + a_3 Q_{IN}^2, \quad (11)$$

where ω_r is the pump speed and a_1, a_2, and a_3 are a set of empirical constants (Isermann 2006, Wolfram 2001, Kallesøe et al. 2006). Similarly, the torque required to produce the head defined in Eq.11 can be specified as

$$\tau_m(t) = b_1\omega_r Q_{IN} + b_2 Q_{IN}^2, \quad (12)$$

where τ_m is the torque and b_1 and b_2 are another set of empirical constants (Isermann 2006, Wolfram 2001, Kallesøe et al. 2006). For a given speed, it is clear that Eqs. 11 and 12 produce curves that are similar to those found in most manufacturer data sheets. Including viscous friction, the net torque is

$$J\frac{\partial\omega_r}{\partial t} = \tau_e - \tau_m - \beta\omega_r, \quad (13)$$

where J is the moment of inertia, τ_e is the torque of electromechanical origin, and β is the coefficient of viscous friction.

The complete simulation model must include the electrical state equations for the three-phase induction machine. In the synchronously rotating d-q reference frame, these equations are (Krause 1986)

$$\frac{\partial\lambda_{ds}}{\partial t} = v_{ds} + \omega\lambda_{qs} - r_s i_{ds}, \quad (14)$$

$$\frac{\partial\lambda_{qs}}{\partial t} = v_{qs} - \omega\lambda_{ds} - r_s i_{qs}, \quad (15)$$

$$\frac{\partial\lambda_{dr}}{\partial t} = v_{dr} + (\omega - p\omega_r)\lambda_{qr} - r_r i_{dr}, \quad (16)$$

and

$$\frac{\partial\lambda_{qr}}{\partial t} = v_{qr} - (\omega - p\omega_r)\lambda_{dr} - r_r i_{qr}. \quad (17)$$

The overall eighth-order model consists of Eqs.8, 9, 10, and 13 through 17. The nomenclature used in the electrical state equations is summarized in Table 2.

TABLE 2: Variables and constants used in the electrical state equations (Eqs. 14 - 17).

Parameter	Definition
λ_{ds}	Direct-axis stator flux
λ_{qs}	Quadrature-axis stator flux
λ_{dr}	Direct-axis rotor flux
λ_{qr}	Quadrature-axis rotor flux
r_s	Stator resistance
r_r	Rotor resistance
i_{ds}	Direct-axis stator current
i_{qs}	Quadrature-axis stator current
i_{dr}	Direct-axis rotor current
i_{qr}	Quadrature-axis rotor current
v_{ds}	Direct-axis stator voltage
v_{qs}	Quadrature-axis stator voltage
v_{dr}	Direct-axis rotor voltage
v_{qr}	Quadrature-axis rotor voltage
p	Number of pole pairs
ω	Frame speed
ω_r	Pump and rotor mechanical speed

The complete system model was simulated using MATLAB. Figure 6 shows both the real electrical power and the pump output flow rate (Q_{IN}) as obtained using a representative set of parameters. Note that the flow rate peaks and then decreases to a steady-state value. This behavior is due primarily to the effects of the micron filters, which are initially empty. Once the filter housing

has filled with water, the pump does not have to supply as much liquid as it did at the outset. In steady state, the pump is primarily supplying the overboard discharge piping.

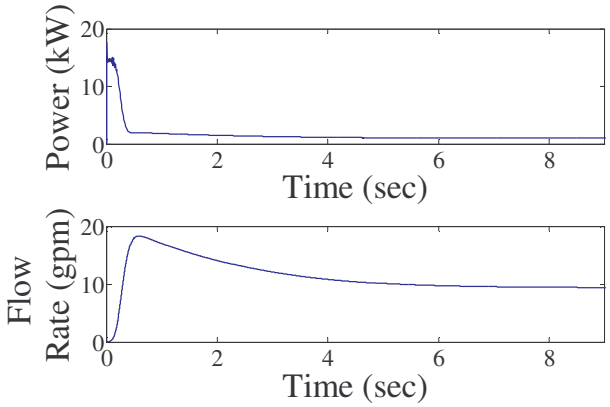

FIGURE 6. Electrical power and pump output flow rate during a typical start. Note that the real power drawn by the motor decreases slowly after the initial inrush.

During the simulated investigations, the fluid capacitance was varied in order to simulate the effect of a clogged filter. The increased capacitance represents the fact that the head across a clogged filter increases even though the stored volume remains essentially constant. Figure 7 shows simulated results obtained for two different filter states. Note that the time required for the real power to reach steady state is considerably longer when the filter is clogged. Such behavior can be detected by a NILM.

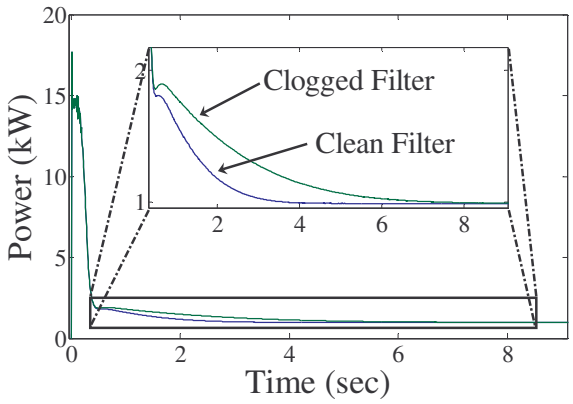

FIGURE 7. Real power drawn by the simulated motor during two different starts. The clog was simulated by changing the fluid capacitance associated with the filters.

MODEL VERIFICATION

In order to verify the simulated results presented previously, experiments were conducted both in the laboratory and aboard two active USCG Cutters. This section summarizes the procedures and results of those experiments.

LABORATORY EXPERIMENTS

For initial investigation a small test stand was constructed in the laboratory. In this setup, which is shown in Fig. 8, the RO startup procedure is simulated by capping the filter discharge piping. This models the blocked-flow effect caused by the secured HP pump before it starts. A 0.10-inch diameter hole was drilled in the cap to vent air during the charging process. A similar bleed outlet is located at the top of the micron filter housing in the systems aboard the Cutters (Village Marine 2004).

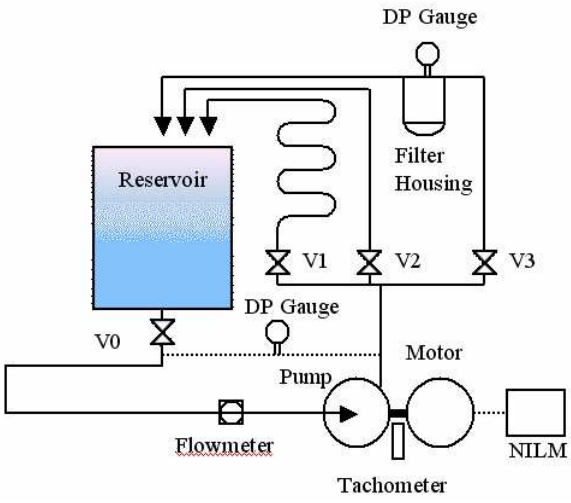

FIGURE 8. Diagram of the laboratory test stand. Note that a NILM monitors the power drawn by the motor.

To simulate the constant discharge flow from the RO unit's cyclone separators, valve V1 on the test stand was partially open during all tests. Valve V3, which leads to the filter housing, was left completely open and valve V2 was left fully closed. As shown in Fig. 8, several key mechanical and hydraulic quantities were measured.

In the laboratory experiments, clogging was simulated by wrapping the filter element with paper towels. These towels were held in place with fiberglass window-screen material and four rubber bands. A total of two paper-towel wraps and six screen wraps were used to represent a fouled filter. Initial testing showed that the filter needed to be completely covered by the fouling material in order to induce a reasonable clogging effect.

Because of the relatively small size of the filter housing in the test stand, the introduction of the fouling material appreciably reduced the amount of open volume that could be filled with water. To ensure consistency, some water needed to be added to the housing before conducting any tests with clean filters.

In the laboratory each test run was initiated by starting the centrifugal pump motor. After running the motor for twelve seconds, it was stopped and the filter housing was drained to the appropriate level. If necessary, the filter condition was then modified for the next experiment.

Four different sets of filter conditions were considered. In the first set, a clean filter was tested. Subsequently, the clean filter was surrounded with the fouling material described previously. For comparison purposes, two other sets of experiments were conducted. In the first of these, no filters were placed in the housing, and in the second, the filter was bypassed by closing valve V3. With V3 closed, the filter housing itself is effectively removed from the system.

Figure 9 shows results obtained with three different sets of filter conditions. Just as predicted by the model, more time is required for the electrical power to reach steady state when the filter is clogged. In addition, note that the "hump" that follows the in-rush period disappears when the filter housing is bypassed. This result supports the claim that filter charging affects the power drawn by the motor.

Figure 10 provides further proof of the validity of the proposed model. That figure shows the measured pump flow rate during each of the experiments considered in Fig. 9. Note that the initial flow rate is considerably higher when the filters are used. Furthermore, a comparison of Fig. 9 and Fig. 10 demonstrates that there is a clear relationship between electrical power and pump flow rate.

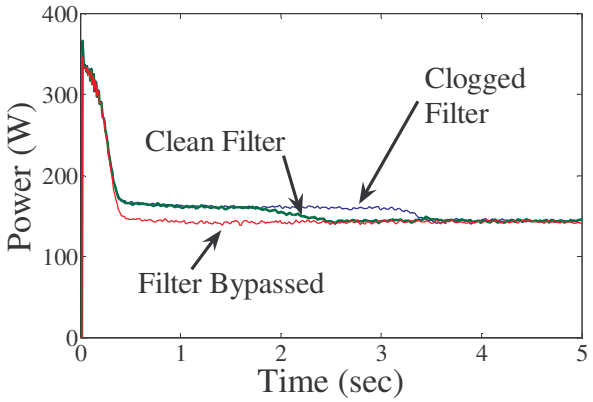

FIGURE 9. Real power flowing into the terminals of the motor in the laboratory test stand. Results obtained with three different sets of filter conditions are shown here.

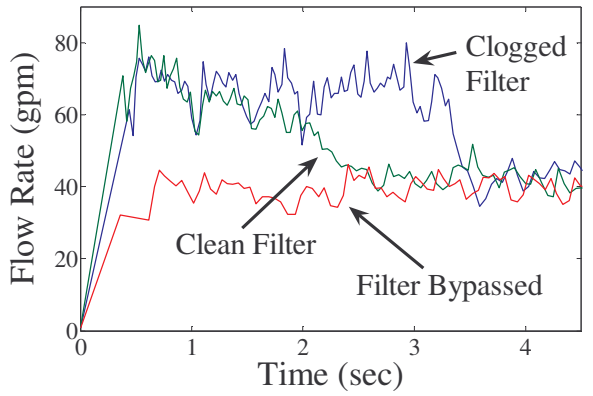

FIGURE 10. Pump output flow rate in the laboratory test stand. Results obtained with three different sets of filter conditions are shown here.

FIELD EXPERIMENTS

To further validate the model, experiments were performed using the RO unit aboard the *USCGC Escanaba*. For complete realism, these experiments followed the start procedure outlined in the RO technical manual (Village Marine 2004). As prescribed by the manufacturer, all pumps were initially secured and the valves were aligned so that water was allowed to bypass the HP pump. To begin the filter charging process,

the operator started the LP pump from the master control console. Once the HP pump inlet pressure had stabilized, the HP bypass valve was closed, causing the membrane pressure to rise into the range between 800 and 1000 psi. Because our experiments were conducted while the ship was in port, all product water was discharged overboard. To allay concerns related to the effects of any initial water in the filter housing, five minutes were allowed to pass between subsequent starts. This waiting period allowed the housings to drain to a consistent state.

Figure 11 shows the two different sets of filters that were used during the initial in-port experiments. The crew of the *Escanaba* graciously saved these elements during a previous cruise. According to the ship's engineering logs, the last recorded pressure across the fouled filter was 18 psi and the last recorded pressure across the clean filter was 4 psi. For reference, the system technical manual recommends filter replacement or cleaning at approximately XX psi (Village Marine 2004).

FIGURE 11. Filters used in the field experiments conducted aboard the *Escanaba*. The filter on the left shows considerable contamination and wear.

Figure 12 again demonstrates how filter condition affects the aggregate power drawn by the LP pump. As shown, the time needed to reach steady state is shorter when the filter is clean. Because the NILM monitors the aggregate power drawn by all of the pumps in the RO system, the HP pumps also affect the measured data shown in Fig. 12. The abrupt change in the power drawn during the clean filter experiment was caused by the start of an HP pump. Although it is not shown in Fig. 12, a similar change occurs in the clogged filter data.

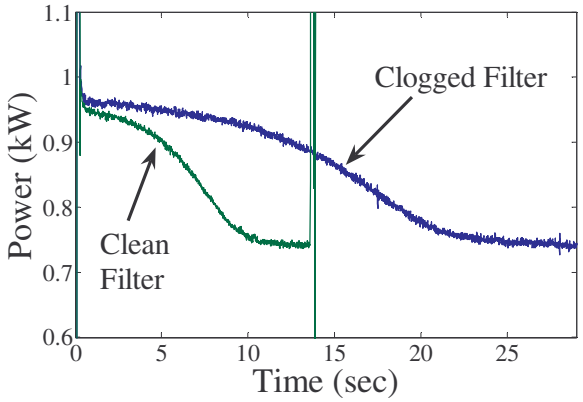

FIGURE 12. Real power drawn by the pumps aboard the *Escanaba* during the in-port experiments. The abrupt change that occurs approximately 14 seconds into the clean filter experiment was caused by the start of an HP pump.

FILTER CONDITION DIAGNOSTICS

The simulated and experimental results presented previously demonstrate that filter condition affects the transient electrical power drawn by the RO unit's LP pump. In particular, the time needed to reach steady state increases as the filter clogs. Filter condition can thus be trended by monitoring the time needed to reach steady state. For convenience, this diagnostic parameter is denoted as the steady-state time.

One way to record the steady-state time is to estimate how long it takes for the slope of the real power to approach zero. This can be accomplished using a numeric approximation to the derivative operator. A typical diagnostic report for an Engineering Officer (EO) would display a plot showing how the steady-state time has varied over the last several starts. A change-of-mean detector could be used to automatically determine if the diagnostic parameter has exceeded a recommended threshold. Suitable

software and alerting capabilities are currently under development.

It is important to note that the proposed diagnostic process requires the use of a consistent startup procedure. Most importantly, the fluid level throughout the system must drain to a consistent initial level. If not, the LP pump would have to move a different volume of fluid during each start, thus causing unwanted and potentially misleading variations in the steady-state time. Additionally, the diagnostic process requires the operator to use a consistent initial valve alignment and a consistent pump start procedure. All of the above criteria can be easily met provided that the system is allowed to drain between subsequent starts and that the operator follows the manufacturer's recommended startup process.

UNDERWAY FIELD RESULTS

To demonstrate the efficacy of the proposed model-based diagnostic indicator, data has been recorded during several recent cruises aboard both the *Seneca* and the *Escanaba*. On each ship, data has been collected on a continuous basis using a single NILM that monitors the aggregate power flowing to all three pumps.

Figure 13 compares the LP pump power recorded during two starts aboard the *Escanaba* on 30 January 2007. These traces were recorded immediately before and after a micron filter replacement. Once again, note that the power stabilizes sooner when the filter is clean.

Figure 14 shows how the measured steady-state time varied onboard the *Escanaba* throughout January 2007. This figure was created by first estimating the steady-state time for each valid start. Between starts 24 and 25, the micron filters were replaced. Note the significant increase that occurred in the days preceding the filter replacement. Such a change is consistent with the pressure readings recorded by the crew. Future diagnostic software will create such plots and provide them to the EO and his staff.

It should be noted that the point-to-point fluctuations shown in Figure 14 are to be expected, as logs indicate that the pressure across the filters varies from watch to watch. These variations are caused by a number of factors, including non-uniform filter fouling and abrupt changes in feed water quality. If necessary, a simple low-pass filter could be used to smooth the data. The ability of the indicator to reject natural fluctuations is a clear demonstration of its robustness.

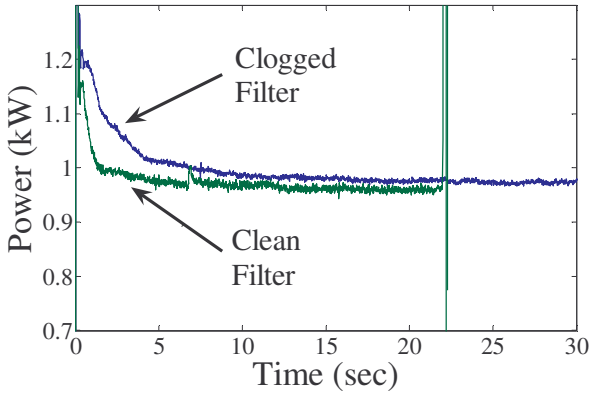

FIGURE 13. Real power drawn by the pumps aboard the *Escanaba* before and after a micron filter replacement. Note that the abrupt change in the clean filter data was caused by the start of an HP pump.

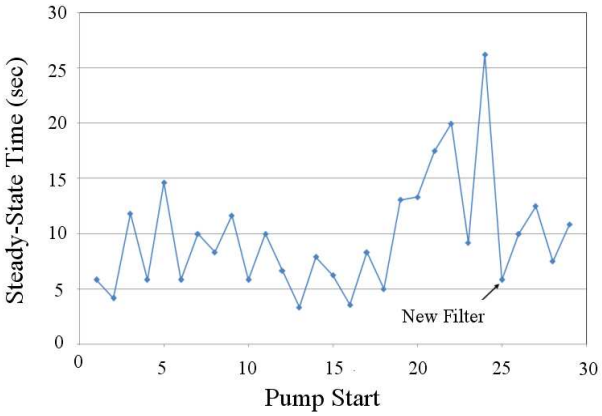

FIGURE 14. Trend in the steady-state start time on the *Escanaba* during January 2007. Note that the filter was replaced between starts 24 and 25.

CONCLUSIONS

The NILM is a rugged, low-cost diagnostic system that is ideally suited to monitor electrical systems such as reverse-osmosis plants. In the

case of RO units, for instance, the diagnostic tools presented in this paper represent only a portion of the NILM's capabilities. Cox et al. (2007) and Mitchell (2007) discuss a number of other faults that can be detected by the NILM, including membrane failures, operator errors, and premature pump wear. The ability of the NILM to identify multiple faults in a single system demonstrates that it can simplify the monitoring and assessment process.

REFERENCES

Armstrong, P., C. Laughman, S. Leeb, and L. Norford. 2006. Detection of rooftop cooling unit faults based on electrical measurements. *HVAC+R Research Journal* 12: 151–175.

Cox, R., J. Mosman, T. McKay, S. Leeb, and T. McCoy. 2006. Diagnostic indicators for shipboard cycling systems using non-intrusive load monitoring. In *Proc. ASNE Day 2006*, June, Arlington, VA.

Cox, R. 2006. Minimally intrusive strategies for fault detection and energy monitoring. Ph.D. diss., Massachusetts Institute of Technology, Cambridge.

Cox, R., M. Piber, G. Mitchell, P. Bennett, J. Paris, W. Wichakool, S. Leeb. 2007. Improving shipboard maintenance practices using non-intrusive load monitoring. In *Proc. ASNE Intelligent Ships Symposium VII*, May, Philadelphia, PA.

DeNucci, T. et al. 2005. Diagnostic indicators for shipboard systems using non-intrusive load monitoring. In *Proc. 1st IEEE Electric Ship Technologies Symposium*, July, Philadelphia, PA.

Hogan, N. 1989. *Modeling, Analysis, and Control of Physical Systems.* Course notes for MIT course 2.151: Advanced System Dynamics and Control, Spring 1991.

Isermann, R. 2006. *Fault-Diagnosis Systems.* Berlin: Springer-Verlag.

Kallesøe, C. V. Cocquempot, R. Izadi-Zamanabadi. 2006. Model based fault detection in a centrifugal pump application. *IEEE Trans. On Control Systems Technology* 14(2): 204-215.

Krause, P., O. Wasynczuk, and S. Sudhoff. 1986. *Analysis of Electric Machinery.* New York: McGraw-Hill.

Laughman, C., P. Armstrong, L. Norford, and S. Leeb, 2006. The detection of liquid slugging phenomena in reciprocating compressors via power measurements. In *Proc. International Compressor Engineering Conference at Purdue*, July, West Lafayette, IN.

Lee, K. 2003. Electric load information system based on non-intrusive power monitoring. Ph.D. diss., Massachusetts Institute of Technology, Cambridge.

Leeb, S. 1993. A conjoint pattern recognition approach to nonintrusive load monitoring. Ph.D. diss., Massachusetts Institute of Technology, Cambridge.

Leeb, S., S. Shaw, and J. Kirtley. 1995. Transient event detection in spectral envelope estimates for nonintrusive load monitoring. *IEEE Trans. on Power Delivery* 10: 1200–1210.

Mitchell, G. 2007. Shipboard fluid system diagnostics using non-intrusive load monitoring. N.E./S.M. thesis, Massachusetts Institute of Technology, Cambridge.

Munson, B., D. Young, T. Okiishi. 1998. *Fundamentals of Fluid Mechanics.* New York: John Wiley and Sons.

Oppenheim, A., A. Willsky, and I. Young. 1988. *Signals and Systems.* Englewood Cliffs, NJ: Addison Wellesley.

Ramsey, J., et al. 2005. Shipboard applications of non-intrusive load monitoring. In *Proc. ASNE Reconfiguration and Survivability Symposium,* February, Atlantic Beach, FL.

Shaw, S. 2000. System identification techniques and modeling for non-intrusive load diagnostics.

Ph.D. diss., Massachusetts Institute of Technology, Cambridge.

Village Marine Tec. 2004**.** *Model RC7000 plus reverse osmosis desalination plant operations and maintenance manual.* Gardena, CA.

Volk, M. 2005. *Pump Characteristics and Applications.* Boca Raton, FL: CRC Press.

Wolfram, A., D. Füssel, T. Brune, and R. Isermann. 2001. Component-based multi-model approach for fault detection and diagnosis of a centrifugal pump. In *Proc. American Control Conference (ACC)*, June, Arlington, VA.

Wood, D. S. Lingireddy, P. Boulos, B. Karney, D. McPherson. 2005. Numerical methods for modeling transient flow in distribution systems. *Journal of the American Water Works Association* 97(7): 104-115.

Zarambo, F. 1992. Desalination plants. In *Marine Engineering*, ed. R. Harrington. Jersey City, NJ: Society of Naval Architects and Marine Engineers.

ACKNOWLEDGMENTS

The authors gratefully acknowledge the assistance and support provided by the crews of the *USCGC Seneca* and the *USCGC Escanaba.* Their patience has been indispensable. This work was supported in part by the Grainger Foundation, the United States Coast Guard, the U.S. Navy through ONR's ESRDC program, and NAVSEA.

Lt. Gregory R. Mitchell, USN *is*

Dr. Robert Cox *received the S.B., M.Eng., and Ph.D. degrees from the Massachusetts Institute of Technology in 2001, 2002, and 2006, respectively. He is currently Assistant Professor of Electrical and Computer Engineering at UNC Charlotte. His research is focused on the design, analysis, and maintenance of electrical actuators, power-electronic drives, analog instrumentation, and sensors.*

James Paris *is a pursuing doctoral degree in Electrical Engineering at MIT.*

Dr. Steven B. Leeb *received the S.B., S.M., E.E. and Ph.D. degrees from MIT. He currently holds appointments as Professor of Electrical Engineering and Professor of Mechanical Engineering at MIT. He is concerned with the design, analysis, and development of all kind of machinery with electrical actuators, sensors, or power-electronic drives.*